Virtual FAS by Learning-Based Imaginary Antennas

Kai-Kit Wong, *Fellow, IEEE*, Chao Wang, *Senior Member, IEEE*, Haibin Zhang, Guo Li, Cheng-Cai Wang, Chan-Byoung Chae, *Fellow, IEEE*, and Ross Murch, *Fellow, IEEE*

***Abstract*—Fluid antenna system (FAS) represents a new technology able to flexibly and instantaneously change the antenna position for optimizing wireless communication performance. The high-resolution adjustment of the antenna position is what makes FAS powerful in taking full advantage of the fading variation in space. To obtain the benefits of FAS but without the complication of implementing FAS, this letter considers a mobile receiver with several fixed-position antennas and employs a transformer-based signal prediction network to deduce the received signals at other positions. This is possible since the received signals are correlated in space. The outcome is an increased dimension multiple-input multiple-output (MIMO) receiver which can be interpreted as a virtual FAS with imaginary antennas. We evaluate the proposed system in multiuser channels and adopt regularized zeroforcing (RZF) in the virtual FAS to deal with the interference. Simulation results demonstrate that the proposed virtual FAS outperforms significantly the original fixed-position MIMO system.**

***Index Terms*—Antenna array, fluid antenna system, imaginary antennas, machine learning, multiuser communications.**

I. Introduction

FLUID ANTENNA system (FAS) represents the concept of antenna position flexibility, thanks to recent advances in software-defined liquid-based antennas [1], [2], surface wave-based flexible antennas [3], [4], and reconfigurable pixel-based antennas [5], [6], [7]. FAS for wireless communications was first introduced by Wong *et al.* for single-user systems in [8] and multiuser systems in [9], [10]. Overview articles can also be found in [11], [12], [13] while [14] discusses some research opportunities. Recent efforts have been made to understand the performance of FAS under different channel environments [15], [16], [17] and how channel state information (CSI) can be estimated in FAS [18], [19], [20]. Moreover, learning-based methods have been presented to optimize the antenna position (a.k.a. port selection) [21] and even jointly with beamforming for integrated sensing and communication (ISAC) applications [22]. It is also worth mentioning the related work under the name of 'movable antennas' that particularly targets deterministic or quasi-static fading channels [23], [24].[1]

Despite the early stage of FAS research, now it is apparent that being able to finely adjust the antenna position is advantageous though the channels at close-by positions are highly correlated. It is typically not advisable to deploy multiple fixed antennas at close-by positions to obtain the benefits of FAS, certainly not if the antennas also come with individual radio frequency (RF) chains. In this context, the research on implementing fluid antennas, encompassing liquid-based and reconfigurable pixel-based technologies, has garnered increasing attention recently [11]. However, each approach possesses different strengths and weaknesses. Consequently, designing a suitable technology to achieve fast switchable ports with high spatial resolution poses a significant challenge. Additionally, reducing response times for switching to meet practical implementation requirements presents another obstacle [8].

Considering the implementation challenges, we attempt to obtain the benefits of FAS using conventional fixed-position antennas without actually needing to deploy FAS. This is possible because the received signals at close-by positions are correlated and hence can be inferred with the knowledge of the correlation structures (i.e., channel side information). However, conventional prediction techniques, such as interpolation or compressed sensing, cannot effectively leverage correlation structures, leading to prediction inaccuracies that fail to meet signal reception requirements [25], [26]. Furthermore, it is worth noting that signal prediction differs from CSI prediction, with the former being notably more intricate. Therefore, the "predictor antenna", as recently introduced in [27] for CSI prediction, is not applicable for signal prediction. Fortunately, the recent advancements in employing deep learning for channel prediction in the physical layer have made it a viable solution [28]. In other words, presumably, it is possible to deploy fixed-position antennas to take signal samples in space, use them to infer the missing signals at other positions and hence increase the dimensionality of the channel (the rank of channel matrix). We regard this system as a virtual FAS with imaginary (non-existing) antennas. The potential is massive. Theoretically, this may mean that the capability of multiple-input multiple-output (MIMO) is no longer limited by the numbers of fixed antennas and RF chains. Virtual FAS transcends the hardware constraint and stretches its capability to an unprecedented level.

The impact of virtual FAS is far-reaching since it propounds to use channel side information (correlation structures in this case) to obtain a fuller signature of the signals in the spatial domain that exceeds the hardware limitation and thus lifts the performance limits that are not known achievable before. The goal of this letter is to illustrate this potential by considering

This work of H. B. Zhang was supported the Defense Industrial Technology Development Program under Grant JCKY2021608B001.

K.-K. Wong is with the Department of Electronic and Electrical Engineering, University College London, London WC1E 6BT, U.K. (e-mail: kai-kit.wong@ucl.ac.uk). He is also affiliated with Yonsei Frontier Laboratory, Yonsei University, Seoul, 03722, Korea.

C. Wang is with the Integrated Service Networks Lab, Xidian University, Xi'an 710071, China (e-mail: drchaowang@126.com).

H. B. Zhang and G. Li are with the School of Cyber Engineering, Xidian University, Xi'an 710071, China (e-mail: liguo@stu.xidian.edu.cn, hbzhang@mail.xidian.edu.cn).

C. C. Wang is with the School of Automation Science and Electrical Engineering, Beihang University, Beijing 100191, China (e-mail: ccwang@pku.edu.cn).

C. B. Chae is with the School of Integrated Technology, Yonsei University, Seoul, 03722, Korea (e-mail: cbchae@yonsei.ac.kr).

R. Murch is with the Department of Electronic and Computer Engineering and Institute for Advanced Study (IAS), Hong Kong University of Science and Technology, Clear Water Bay, Hong Kong SAR, China.

Corresponding authors: Chao Wang and Kai-Kit Wong.

[1]FAS includes all forms of movable and non-movable position-flexible antennas so movable antenna system can be viewed as a subclass of FAS.

as an example the interference channel where a fixed-position MIMO receiver handles more interferers than its antennas via virtual FAS. Our contributions are listed as follows.

- This is the first work to study virtual FAS. In particular, we propose a transformer-based signal prediction network to exploit the correlation structures amongst the received signals at multiple positions (or ports) to infer the unobserved signals in space. A virtual FAS (or an increased dimension MIMO channel) is then formed with both the observed and inferred received signals for processing.
- We consider the use of regularized zeroforcing (RZF) on the virtual FAS channel to tackle the interference. We are particularly interested in the situations where the number of interferers exceeds that of the physical antennas.
- Simulation results demonstrate superior performance of the proposed virtual FAS over the original fixed-position MIMO system in terms of bit-error-rate (BER).

Notations: $(\cdot)^T$, $(\cdot)^H$, and $\|\cdot\|_2$ denote the transpose, the conjugate transpose, and the L_2 norm of a matrix; $\mathbb{R}^{n\times n}/\mathbb{C}^{n\times n}$ stands for an $n\times n$ real/complex matrix; $\mathbf{x}\sim\mathcal{CN}(\mathbf{\Lambda},\mathbf{\Delta})$ represents the circularly symmetric complex Gaussian vector having a mean vector of $\mathbf{\Lambda}$ and covariance matrix of $\mathbf{\Delta}$. $\Re(a)$ and $\Im(a)$ denote its real and imaginary parts, respectively.

II. System Model

A. Virtual FAS

Consider a downlink multiuser system where a MIMO base station (BS) transmits information-bearing signals to K user equipments (UEs) on the same time-frequency resource block. The BS has K fixed antennas, each of which is dedicated to transmitting one UE's signal without precoding. CSI at the BS is therefore not needed. Each UE has $M(<K)$ fixed-position antennas spread over a one-dimensional (1D) prescribed space of length $W\lambda$ where λ denotes the wavelength.

The signal received at the ℓ-th fixed-position antenna of the k-th UE is given by

$$y_\ell^{(k)} = h_\ell^{(k,k)} s_k + \sum_{\substack{j=1\\ j\neq k}}^{K} h_\ell^{(j,k)} s_j + n_\ell^{(k)}, \ell = 1,\ldots,M, \quad (1)$$

where $s_k\sim\mathcal{CN}\left(0,\sigma_s^2\right)$ represents the signal intended to UE k, $h_\ell^{(j,k)}$ is the channel from the j-th BS antenna to the ℓ-th antenna of UE k, and $n_\ell^{(k)}\sim\mathcal{CN}\left(0,\sigma_n^2\right)$ denotes the received noise at the ℓ-th antenna of UE k. Apparently, $\sum_{j\neq k} h_\ell^{(j,k)} s_j$ is the interference on the signal reception at UE k.

As $M<K$, the UEs do not have enough degree of freedom (DoF) to handle their interference and would struggle. In [9], [10], it was proposed to adopt FAS at each UE which would allow it to receive the signals at the position where the overall interference suffers from deep fade and hence disappears. This nonetheless requires a position-flexible FAS to be deployed at each UE, which is not available in the model of this letter.

Without the FAS hardware, in fact, it is actually possible to still benefit from the concept of FAS. In particular, one core feature of FAS is that it always deals with correlated signals in space because the received signals at close-by positions are highly correlated. This reminds us that we can have not only the received signals at those fixed positions but also something in between due to the correlation structure. The novelty of this work is to exploit the inherent correlation and establish the signals in between the fixed-position antennas. The outcome is at each UE, a MIMO receiver with increased dimension which we refer to it as a virtual FAS with imaginary antennas.

We leave the details of how the received signals at imaginary positions can be predicted in Section III. Now, assuming that UE k predicts the signals received at N_p imaginary positions based on the signals received at M fixed-position antennas to obtain a vector of $N=M+N_p$ signals, we denote $\boldsymbol{u}_k = [u_1^{(k)}\cdots u_M^{(k)}]^T$ as the actual positions of the fixed antennas[2] and $\boldsymbol{q}_k = [q_1^{(k)}\cdots q_{N_p}^{(k)}]^T$ as the positions of the imaginary (non-existing) antennas. Furthermore, we denote the transmit signal vector as $\mathbf{s}=[s_1\cdots s_K]^T$. Then the overall received signals (both observed and predicted ones) in vector form can be written as

$$\mathbf{y}_k \triangleq \begin{bmatrix}\mathbf{y}_k^{\rm ob}\\ \mathbf{y}_k^{\rm un}\end{bmatrix} = \underbrace{\begin{bmatrix}\mathbf{H}_k^{\rm ob}(\boldsymbol{u}_k)\\ \mathbf{H}_k^{\rm un}(\boldsymbol{q}_k)\end{bmatrix}}_{\triangleq\mathbf{H}_k}\mathbf{s} + \begin{bmatrix}\mathbf{n}_k^{\rm ob}\\ \mathbf{n}_k^{\rm un}\end{bmatrix}, \quad (2)$$

where $\mathbf{y}_k^{\rm ob}$ and $\mathbf{y}_k^{\rm un}$ represent the observed signals of the fixed-position antennas and the predicted signals of the imaginary antenna positions, respectively, $\mathbf{H}_k^{\rm ob}(\cdot)$ and $\mathbf{H}_k^{\rm un}(\cdot)$ denote the respective channel matrices, $\mathbf{n}_k^{\rm ob}$ is the usual additive Gaussian noise vector at the received fixed-position antennas and $\mathbf{n}_k^{\rm un}$ is the additive prediction noise at the imaginary antennas.[3]

Consequently, we now have an increased dimension MIMO channel for UE k, from $M\times K$ to $N\times K$ where $N=M+N_p>M$. The objective is to have $N\geq K$ so that UE k can then perform RZF to effectively recover the message

$$\hat{s}_k = \mathbf{e}_k^T\left(\mathbf{H}_k^H\mathbf{H}_k+\beta_k\mathbf{I}_K\right)^{-1}\mathbf{H}_k^H\mathbf{y}, \quad (3)$$

where β_k is the regularizing factor, $\mathbf{I}_K$ denotes an $K\times K$ identity matrix, and $\mathbf{e}_k$ is the k-th column of $\mathbf{I}_K$.

B. Channel Model

As in [24], we adopt a multi-path geometric channel model. Under this model, the channel is determined by the angle-of-departures (AoDs), angle-of-arrivals (AoAs), and gains of all the paths. At different antenna positions, the phases of channel path are different due to propagation delay. If there are L_k scatterers between the BS and UE k, then the corresponding channel vector can be constructed as

$$\mathbf{H}_k^{\rm ob}(\boldsymbol{u}_k) = \mathbf{G}_k^H(\boldsymbol{u}_k)\mathbf{\Sigma}_k\mathbf{F}_k, \quad (4)$$

where $\mathbf{F}_k\triangleq[\mathbf{f}_1;\mathbf{f}_2;\ldots;\mathbf{f}_{L_k}]$ and $\mathbf{\Sigma}_k\in\mathbb{C}^{L_k\times L_k}$ denotes the fading coefficient matrix from the transmit reference point to

[2]While the antenna positions in a random situation are arbitrary, traditionally, the fixed antennas are located with a 0.5λ spacing to ensure sufficient diversity in rich-scattering environments. However, it is noteworthy that this same old rule-of-thumb may be less effective than placing the fixed antennas with a closer spacing because correlation helps the prediction of the received signals in between the fixed positions. This letter will not attempt to find the answer of what is the best antenna spacing but defer this to future work.

[3]Though a larger N_p gives a higher spatial degree of freedom, it increases the prediction noise $\mathbf{n}_k^{\rm un}$ due to higher estimation inaccuracy. Determining the optimal N_p necessitates evaluating the trade-off between degrees of freedom and the prediction noise power, a topic beyond the scope of this paper.

This article has been accepted for publication in IEEE Wireless Communications Letters. This is the author's version which has not been fully edited and content may change prior to final publication. Citation information: DOI 10.1109/LWC.2024.3382220

the receive reference point [24]. In particular, taking the left endpoint at the BS as the transmit reference point, we have

$$\mathbf{f}_l \triangleq \left[1, e^{-j\frac{2\pi d}{\lambda}\sin(\theta_{t,l}^k)}, \ldots, e^{-j\frac{2(K-1)\pi d}{\lambda}\sin(\theta_{t,l}^k)}\right] \quad (5)$$

as the transmit steering vector of the l-th path, in which d is the inter-element spacing of the BS antennas and $\theta_{t,l}^k$ is the corresponding AoD. Similarly, we also have

$$\mathbf{G}_k(\boldsymbol{u}_k) \triangleq [\mathbf{g}_1(\boldsymbol{u}_k), \mathbf{g}_2(\boldsymbol{u}_k), \ldots, \mathbf{g}_{L_k}(\boldsymbol{u}_M)], \quad (6)$$

where $\mathbf{g}_k(\boldsymbol{u}_j) \triangleq \left[1, e^{-j\frac{2\pi u_1^{(k)}}{\lambda}\sin(\theta_{r,l}^k)}, \ldots, e^{-j\frac{2\pi u_M^{(k)}}{\lambda}\sin(\theta_{r,l}^k)}\right]^T$ is the receive steering vector of UE k for the l-th path and $\theta_{r,l}^k$ is the corresponding AoA of that channel path.

III. Deep Learning Aided Signal Prediction

We will use a deep learning approach to predict the signals received at the N_p imaginary antenna positions. Below we first introduce the framework of learning-aided signal prediction, and then show the architecture of the proposed transformer-induced deep neural prediction network (TDNP-Net).

A. Signal Prediction Framework

Given that the available space at a UE is rather limited, the received signals at the N positions are highly correlated. This is particularly true if L_k is not large. Thus, signal prediction becomes possible. However, if the number of predicted positions is large, then neither spatial interpolation methods [25] nor compressed sensing approaches [26] will be effective to enable virtual FAS, due to huge computational complexity and storage demands. As an alternative, we resort to supervised learning to develop data-driven approaches for predicting the signals received at the imaginary positions.

In this letter, we assume that CSI is known as it has been addressed in [19]. In what follows, pilots can be employed to construct the training data set. Specifically, in the i-th training epoch, the true pilots received at the N_p imaginary positions of UE k are denoted as $\mathbf{y}_k^{\mathrm{un},[i]}$ while the corresponding observed signals at the fixed-position antennas are denoted by $\mathbf{y}_k^{\mathrm{ob},[i]}$. As such, the unobserved signals can be predicted as

$$\hat{\mathbf{y}}_k^{\mathrm{un},[i]} = g_{\mathbf{w}}\left(\mathbf{y}_k^{\mathrm{ob},[i]}, \mathbf{H}_k\right), \quad (7)$$

where $g_{\mathbf{w}}(\cdot)$ denotes the TDNP-Net whose network parameter is $\mathbf{w}$. Based on this, the prediction loss of T training samples is adopted as the cost function to optimize the parameters of TDNP-Net using gradient backpropagation, given by

$$J(\mathbf{w}) = \frac{1}{TK}\sum_{k=1}^{K}\sum_{i=1}^{T}\left\|g_{\mathbf{w}}\left(\mathbf{y}_k^{\mathrm{ob},[i]}, \mathbf{H}_k\right) - \mathbf{y}_k^{\mathrm{un},[i]}\right\|_2^2. \quad (8)$$

B. Proposed Architecture

As illustrated in Fig. 1, the proposed TDNP-Net employs a standard encoder-decoder architecture. The encoder, consisting of observed information embedding network (OIEN) and unobserved information embedding network (UIEN), generates latent vectors for observed and unobserved ports, which are concatenated to form a global latent matrix $\mathbf{Y}_k$. The decoder network then reconstructs signals for each port using $\mathbf{Y}_k$. We detail the architectures below.

1) *OIEN*: The OIEN comprises a trainable position embedding matrix $\mathbf{B} \in \mathbb{C}^{256\times N}$, two information embedding modules and a vision transformer (ViT) module. We first adopt multi-layer perception (MLP) to learn the latent representations of the CSI and the received signals of the M observed fixed positions, i.e.,

$$\begin{aligned}\hat{\mathbf{H}}_k^{\mathrm{ob}} &= \mathbf{W}^{\mathrm{H}}\left[\mathcal{R}\left(\mathbf{H}_k^{\mathrm{ob}}(\boldsymbol{u}_k)\right); \mathcal{I}\left(\mathbf{H}_k^{\mathrm{ob}}(\boldsymbol{u}_k)\right)\right]^T + \mathbf{B}^{\mathrm{H}},\\ \mathbf{A}_k &= \mathbf{W}^{\mathrm{y}}\left[\mathcal{R}\left(\left(\mathbf{y}_k^{\mathrm{ob}}\right)^T\right); \mathcal{I}\left(\left(\mathbf{y}_k^{\mathrm{ob}}\right)^T\right)\right] + \mathbf{B}^{\mathrm{y}}, \quad (9)\end{aligned}$$

in which $\mathbf{W}^{\mathrm{H}} \in \mathbb{R}^{256\times 2K}$, $\mathbf{B}^{\mathrm{H}} \in \mathbb{R}^{256\times M}$, $\mathbf{W}^{\mathrm{y}} \in \mathbb{R}^{256\times 2}$ and $\mathbf{B}^{\mathrm{y}} \in \mathbb{R}^{256\times M}$ are the trainable parameters of MLP. Then, a trainable parameter, $\mathbf{B}$, is introduced, whose column vector represents the latent information of each port, such as position. Accordingly, the sub-matrix of $\mathbf{B}$, i.e., $\tilde{\mathbf{B}}_k^{\mathrm{ob}} \in \mathbb{R}^{256\times M}$ represents the latent vectors of M observed positions. Furthermore, the summation of latent representations of signal, positions and CSI, i.e., $\mathbf{X}_k = \mathbf{A}_k + \tilde{\mathbf{B}}_k^{\mathrm{ob}} + \hat{\mathbf{H}}_k^{\mathrm{ob}}$, is input into the ViT module[4] to extract composite features, yielding $\hat{\mathbf{X}}_k \in \mathbb{R}^{256\times M}$. Finally, we use $\hat{\mathbf{X}}_k$ to construct the composite features $\mathbf{Z}_k$, which is given by

$$\mathbf{Z}_k = \begin{cases}\hat{\mathbf{X}}_k, & \text{for observed positons},\\ \mathbf{0}, & \text{for unobserved positions}.\end{cases} \quad (10)$$

2) *UIEN*: We first introduce a learnable token matrix $\hat{\mathbf{B}} \in \mathbb{R}^{256\times N}$, whose column vector represents the embedding information of the FAS's position. Additionally, $\tilde{\mathbf{B}}_k^{\mathrm{un}} \in \mathbb{R}^{256\times N}$ is a masked version of $\hat{\mathbf{B}}$, which retains the embedding information for the N_p unobserved positions while setting others as zeroes. Then, the CSI latent representation of the unobserved positions is extracted using the same MLP in OIEN, which is filled into the sparse matrix $\mathbf{M}_k \in \mathbb{R}^{256\times N}$, i.e.,

$$\hat{\mathbf{H}}_k^{\mathrm{un}} = \mathbf{W}^{\mathrm{H}}\left[\mathcal{R}\left(\mathbf{H}_k^{\mathrm{un}}(\boldsymbol{q}_k)\right); \mathcal{I}\left(\mathbf{H}_k^{\mathrm{un}}(\boldsymbol{q}_k)\right)\right]^T + \mathbf{b}^{\mathrm{H}}, \quad (11)$$

$$\mathbf{M}_k = \begin{cases}\mathbf{0}, & \text{for observed positions},\\ \hat{\mathbf{H}}_k^{\mathrm{un}}, & \text{for unobserved positions}.\end{cases} \quad (12)$$

Finally, we compute the summation of $\mathbf{Y}_k \in \mathbb{R}^{256\times N} = \tilde{\mathbf{B}}_k^{\mathrm{un}} + \mathbf{M}_k + \mathbf{Z}_k$ as the input of the decoder network for predicting the signals at the imaginary positions.

3) *Decoder Network:* The decoder employs a residual network architecture, which includes 2D convolution modules, layer normalization modules, and Gaussian error linear units (GELU) activation function. The decoder network predicts the unobserved signals at the imaginary positions $\hat{\mathbf{Y}} \in \mathbb{C}^{2\times N}$ based on the composite features $\mathbf{Y}_k$. Note that during 2D convolution, $\mathbf{Y}_k$ is considered as an image of size $N \times 1$ with 256 channels.

We employ the Big-O notation for complexity analysis. The computational load of OIEN and UIEN primarily lies in the MLP and multi-head attention mechanism, with com-

[4]Although traditional deep neural networks have been widely used to extract wireless signal features, the emerging network architecture "transformer" has shown greater advantage than traditional architectures in language processing and computer vision tasks. The transformer architecture is specifically designed with the self-attention mechanism, providing it with an expansive receptive field. Moreover, the multi-head mechanism allows the network to concentrate on several distinct areas within the input data.

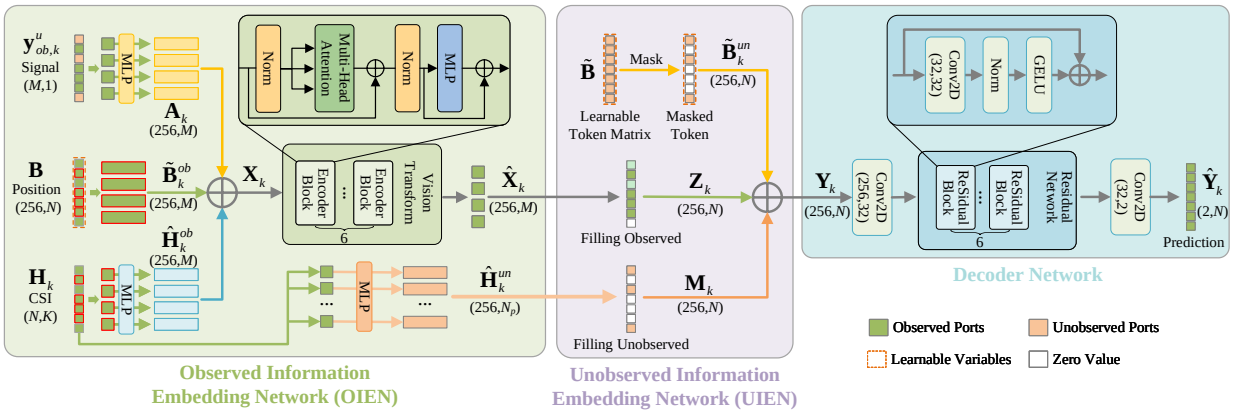

Fig. 1. The proposed learning-aided signal prediction network.

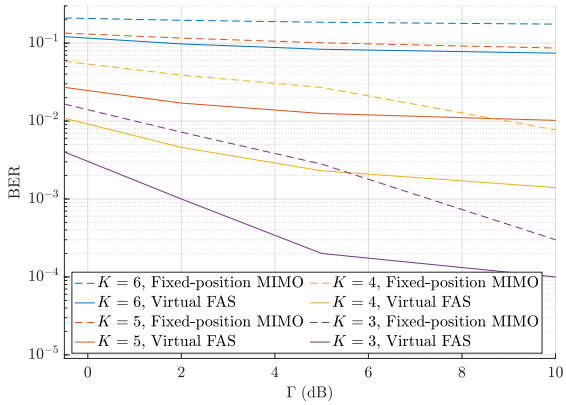

Fig. 2. BER results against SNR with $M = 4$.

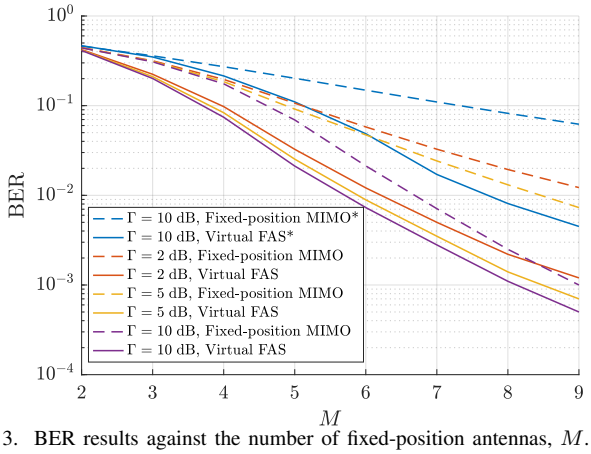

Fig. 3. BER results against the number of fixed-position antennas, M. The "*" symbols mark the simulation results based on the 3GPP clustered delay line (CDL) channel model using the MATLAB 5G toolbox at 24.25 GHz.

plexities of $\mathcal{O}(NK)$ and $\mathcal{O}(N^2)$, respectively. The decoder's computational load mainly resides in the convolutional layers, with a complexity of $\mathcal{O}(N)$. Consequently, the computational complexity of TDNP-Net is $\mathcal{O}(NK + N^2)$.

IV. Simulation Results

In this section, we evaluate the performance of virtual FAS using Monte Carlo simulations. Unless specified otherwise, the carrier frequency $f_c = 3.4$ GHz, the number of users is $K = 6$, the number of antenna positions is $N = 10$, and the number of scatterers is $L_k = 10$, for $1 \le k \le K$ and the signal-to-noise ratio (SNR) is defined as $\Gamma \triangleq \sigma_s^2/\sigma_n^2$. Also, it is assumed that $W = 2$. We use exhaustive search to optimize the regularizing factor β_k for minimizing the BER of each UE. We compare the proposed virtual FAS with MIMO with M fixed-position antennas for different values of M. The model training consists of two stages: pre-training and fine-tuning, both utilizing the AdamW optimizer. During the pre-training stage, the model is trained with a batch size of 32, a learning rate of 0.001, under $\Gamma = 3\,\mathrm{dB}$, and $M = 6$. For fine-tuning, a dynamic number of M is used with a learning rate of 0.0001. Note that $N = 10$ is fixed so the value of N_p is set according to M. In addition, the position vectors $\{\boldsymbol{u}_k, \boldsymbol{q}_k\}$ are randomly generated in over $10,000$ independent channel simulations.

Fig. 2 shows the BER results of the proposed virtual FAS and fixed-position MIMO and compares them. Since $M = 4$, traditional fixed-position MIMO can only support at most 4 users without inter-user interference utilizing RZF. Our virtual FAS predicts the received signals to increase the DoF so that more users can be accommodated. As we can see, virtual FAS can achieve much better performance than traditional MIMO. The impressive performance continues with the increasing K until $K = 5$. However, when $K = 6$, the improvement appears to reduce due to errors in signal prediction.

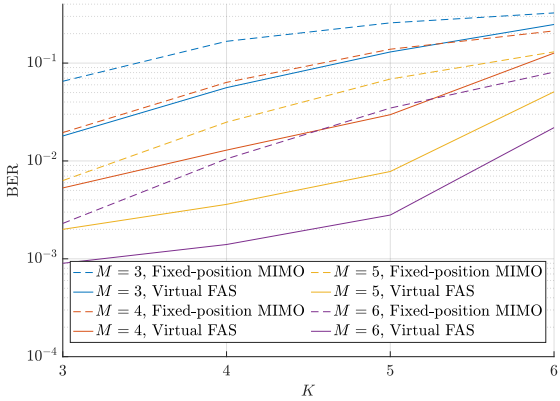

Fig. 4. BER results against the number of users, K with $\Gamma = -1$ dB.

Now, our attention turns to the BER results as M changes in Fig. 3. The results demonstrate that increasing M enlarges the performance gap between virtual FAS and traditional MIMO because increasing M clearly improves the quality of signal prediction due to more observations. Besides, increasing the SNR, Γ, reduces the performance gap, since increasing Γ will improve the signal reception and reduce the benefit brought by the signal prediction of virtual FAS.

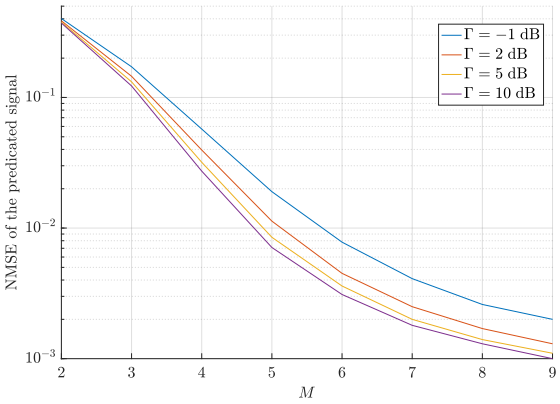

Fig. 5. NMSE against the number of fixed-position antennas, M.

Fig. 4 provides the BER results with the number of users, K, on the x-axis. As has been mentioned above, increasing M will improve signal reception due to the increasing number of observed antenna positions. Therefore, a larger M will result in a smaller BER. Besides, increasing K deteriorates BER due to the increasing inter-user interference. Moreover, increasing M will increase the gains brought by the proposed virtual FAS, which confirms the simulation results given in Fig. 3.

Finally, Fig. 5 shows the prediction accuracy of the signals at the imaginary antenna positions in terms of the normalized mean square error (NMSE). Apparently, increasing M and Γ can both improve the signal estimation accuracy due to more available information. Besides, when $M \geq 4$, the NMSE of signal prediction decreases below 10^{-1}, which achieves much better estimation of the unobserved signals.

V. Conclusion

This letter proposed a virtual FAS with imaginary antennas that increased the dimensionality of fixed-position MIMO by using a deep learning approach. We achieved this by adopting a ViT transformer-based signal prediction network to deduce the signals that would have been received at some imaginary positions in between the fixed antenna positions, due to spatial correlation. Simulation results demonstrated that virtual FAS can greatly enhance the performance of fixed-position MIMO and enable the system to support more users. An important message in this work is that the performance of MIMO is no longer limited by the numbers of fixed-position antennas and RF chains. With spatial correlation as side information, the rank or dimensionality of the channel is higher and MIMO in the form of virtual FAS is a more powerful scheme.

References

[1] Y. Huang, L. Xing, C. Song, S. Wang, and F. Elhouni, "Liquid antennas: Past, present and future," *IEEE Open J. Antennas & Propag.*, vol. 2, pp. 473–487, Mar. 2021.

[2] C. Borda-Fortuny, L. Cai, K. F. Tong, and K. K. Wong, "Low-cost 3D-printed coupling-fed frequency agile fluidic monopole antenna system," *IEEE Access*, vol. 7, pp. 95058–95064, Jul. 2019.

[3] Y. Shen, K.-F. Tong, and K. K. Wong, "Radiation pattern diversified double-fluid-channel surface-wave antenna for mobile communications," in *Proc. IEEE-APS Topical Conf. Antennas & Propag. Wireless Commun. (APWC)*, pp. 085–088, 5-9 Sept. 2022, Cape Town, South Africa.

[4] H. Wang, Y. Shen, K.-F. Tong, and K. K. Wong, "Continuous electrowetting surface-wave fluid antenna for mobile communications," in *Proc. IEEE Region 10 Conference (TENCON)*, 1-4 Nov. 2022, Hong Kong.

[5] B. A. Cetiner *et al.*, "Multifunctional reconfigurable MEMS integrated antennas for adaptive MIMO systems," *IEEE Commun. Mag.*, vol. 42, no. 12, pp. 62–70, Dec. 2004.

[6] A. Grau Besoli, and F. De Flaviis, "A multifunctional reconfigurable pixeled antenna using MEMS technology on printed circuit board," *IEEE Trans. Antennas & Propag.*, vol. 59, no. 12, pp. 4413–4424, Dec. 2011.

[7] L. Jing, M. Li, and R. Murch, "Compact pattern reconfigurable pixel antenna with diagonal pixel connections," *IEEE Trans. Antennas & Propag.*, vol. 70, no. 10, pp. 8951–8961, Oct. 2022.

[8] K.-K. Wong, A. Shojaeifard, K.-F. Tong, and Y. Zhang, "Fluid antenna systems," *IEEE Trans. Wireless Commun.*, vol. 20, no. 3, pp. 1950–1962, Mar. 2021.

[9] K. K. Wong, and K. F. Tong, "Fluid antenna multiple access," *IEEE Trans. Wireless Commun.*, vol. 21, no. 7, pp. 4801–4815, Jul. 2022.

[10] K.-K. Wong, D. Morales-Jimenez, K.-F. Tong, and C.-B. Chae, "Slow fluid antenna multiple access," *IEEE Trans. Commun.*, vol. 71, no. 5, pp. 2831–2846, May 2023.

[11] K.-K. Wong, K.-F. Tong, Y. Shen, Y. Chen, and Y. Zhang, "Bruce Lee-inspired fluid antenna system: Six research topics and the potentials for 6G," *Front. Commun. Net.*, vol. 3, pp. 1–31, Mar. 2022.

[12] K.-K. Wong, W. K. New, X. Hao, K.-F. Tong, and C.-B. Chae, "Fluid antenna system—part I: Preliminaries," *IEEE Commun. Lett.*, vol. 27, no. 8, pp. 1919–1923, Aug. 2023.

[13] J. Zheng *et al.*, "Flexible-position MIMO for wireless communications: Fundamentals, challenges, and future directions," arXiv preprint arXiv: 2308.14578[cs.IT], Nov. 2023.

[14] K.-K. Wong, K.-F. Tong, and C.-B. Chae, "Fluid antenna system—part II: Research opportunities," *IEEE Commun. Lett.*, vol. 27, no. 8, pp. 1924–1928, Aug. 2023.

[15] C. Psomas, P. J. Smith, H. A. Suraweera and I. Krikidis, "Continuous fluid antenna systems: Modeling and analysis," *IEEE Commun. Lett.*, vol. 27, no. 12, pp. 3370–3374, Dec. 2023.

[16] J. D. Vega-Sánchez, A. E. López-Ramírez, L. Urquiza-Aguiar and D. P. M. Osorio, "Novel expressions for the outage probability and diversity gains in fluid antenna system," *IEEE Wireless Commun. Lett.*, early access doi:10.1109/LWC.2023.3329780.

[17] P. D. Alvim *et al.*, "On the performance of fluid antennas systems under α-μ fading channels," *IEEE Wireless Commun. Lett.*, early access doi: 10.1109/LWC.2023.3322106.

[18] C. Skouroumounis and I. Krikidis, "Fluid antenna with linear MMSE channel estimation for large-scale cellular networks," *IEEE Trans. Commun.*, vol. 71, no. 2, pp. 1112–1125, Feb. 2023.

[19] H. Xu *et al.*, "Channel estimation for FAS-assisted multiuser mmWave systems," accepted in *IEEE Commun. Lett.*, 2024.

[20] Z. Zhang, J. Zhu, L. Dai, and R. W. Heath Jr, "Successive Bayesian reconstructor for channel estimation in fluid antenna systems," arXiv preprint arXiv:2312.06551v3, Jan. 2024.

[21] J. Zou, S. Sun and C. Wang, "Online learning-induced port selection for fluid antenna in dynamic channel environment," *IEEE Wireless Commun. Lett.*, early access doi:10.1109/LWC.2023.3328420.

[22] C. Wang *et al.*, "Fluid antenna system liberating multiuser MIMO for ISAC via deep reinforcement learning," *IEEE Trans. Wireless Commun.*, Accepted for publication, 2024. Available on: https://drive.google.com/file/d/1kbHDQMIglS1aVHzjtlpqQLJUaD3dZalr/view?usp=sharing.

[23] L. Zhu, W. Ma and R. Zhang, "Movable-antenna array enhanced beamforming: Achieving full array gain with null steering," *IEEE Commun. Lett.*, vol. 27, no. 12, pp. 3340–3344, Dec. 2023.

[24] L. Zhu, W. Ma, B. Ning and R. Zhang, "Movable-antenna enhanced multiuser communication via antenna position optimization," *IEEE Trans. Wireless Commun.*, doi:10.1109/TWC.2023.3338626.

[25] M. Yalçın and A. Akan, "Interpolation techniques for OFDM channel estimation," in *Proc. IEEE Sig. Process. Commun. Appl. Conf.*, pp. 272–275, 22-24 Apr. 2010, Diyarbakir, Turkey.

[26] S. Uehashi, Y. Ogawa, T. Nishimura, and T. Ohgane, "Prediction of time-varying multi-user MIMO channels based on DOA estimation using compressed sensing," *IEEE Trans. Veh. Tech.*, vol. 68, no. 1, pp. 565–577, Jan. 2019.

[27] J. K. Zheng, J. Y. Zhang, H. Y. Du, D. Niyato, B. Ai, M. Debbah, and K. B. Letaief, "Mobile cell-free massive MIMO: Challenges, solutions, and future directions," *IEEE Wireless Commun., Accepted*, 2024.

[28] A. Kulkarni, A. Seetharam, A. Ramesh, and J. D. Herath, "Deepchannel: Wireless channel quality prediction using deep learning," *IEEE Trans. Veh. Technol.*, vol. 69, no. 1, pp. 443–456, Jan. 2020.